Monte Carlo simulations of polymer brushes

C.-M. Chen and Y.-A. Fwu
Physics Department, National Taiwan Normal University, Taipei, Taiwan
(Received 4 July 2000; published 20 December 2000)

Three-dimensional Monte Carlo simulations of flexible and semiflexible polymer brushes at various grafting densities are carried out to study their equilibrium structure and attendant properties by using the bond fluctuation model. Our simulation results of long flexible polymer brushes are, in general, consistent with predictions of the self-consistent field theory. However, a depletion layer near the substrate is only observed at small grafting densities but not at medium densities. We have also measured the brush height and end-to-end distance of various polymer brushes, and their dependence on grafting density, chain length, and chain stiffness are obtained. The distribution of bending angles at various temperatures are calculated for four different forms of bending energy and our simulation results agree with theoretical predictions very well. Moreover, we study the isotropic-to-nematic transition of polymer brushes, which is found to be a continuous phase transition from our simulation results. Finally, we discuss the effects of local grafting density fluctuation on the monomer and end density distributions.

DOI: 10.1103/PhysRevE.63.011506 PACS number(s): 61.25.Hq, 64.60.−i, 83.10.Rs

I. INTRODUCTION

Polymer chains can be end grafted onto a surface to form a polymer brush which could have important applications in various different problems of lubrication, colloidal stability, adhesion, and biotechnology [1]. For example, polymer brush coated lipid vesicles can be used for controlled drug delivery, in which polymer chains can protect the vesicles from the attack of the immune system. Such brushes have attracted much theoretical [2–5], computational [6,7], and experimental [8,9] attention in recent years. Most theoretical considerations have concentrated on the properties of flexible polymer brushes tethered to a flat [2–4] or a curved surface [10,11] based on models that describe directionally isotropic interactions in the long chain limit of flexible polymers. Various approximation schemes have been employed to calculate the brush height and density profile of polymer brushes, such as Flory-type mean field arguments [2,3] and self-consistent-field (SCF) methods [4]. Among these different approaches, the predictions of SCF methods seem to be in better agreement with numerical results from lattice or off-lattice simulations and experimental observations by neutron scattering techniques. However most previous studies on polymer brushes by computer simulations or experiments are limited to brushes of low grafting densities due to finite computation time or difficulties in preparing samples. Until recently experiments have been performed to study brushes with higher densities using a thermally sensitive poly(*N*-isopropylacrylamide) microgel as the substrate which shrinks at high temperatures (critical solution temperature is about 32 °C) leading to a decrease in its surface area about 10 times [9]. It is also more available now to do intensive simulations using a cluster of dual CPU Linux PC workstations.

Flexible polymers are usually represented by a bead-spring model [12] in which the isotropic interactions between monomers are considered and the interactions between springs are ignored. The equilibrium structure and attendant properties of these flexible polymer brushes are now very well understood. For many synthetic and biological polymers (such as DNA and actin filaments), the backbone structures of these polymers are less flexible or more persistent. Instead of the bead-spring model, these systems can be better represented by a series of connected rigid rods whose length is roughly the persistent length of polymer chains [5,13]. In this case, the interactions between rods of different chains and those on the same chain are in general orientation dependent. An isotropic-to-nematic phase transition [5] is expected as the strength of interactions varies.

In this paper, we will study the equilibrium structure and attendant properties of flexible and semiflexible polymer brushes by three-dimensional Monte Carlo simulations using the bond-fluctuation model. The method of Monte Carlo simulations for the bond-fluctuation model is described in Sec. II. In Sec. III, the equilibrium structure and attendant properties of polymer brushes are investigated for various chain lengths, grafting densities, and chain stiffness, such as the brush height, monomer density profile, and end-segment distribution. A detailed investigation of the distribution of bending angles for four different forms of bending energy is given in Sec. IV. In Sec. V, we discuss the isotropic-to-nematic phase transition of polymer brushes as the chain stiffness, grafting density, or chain length are varied. The effects of local grafting density fluctuation are discussed in Sec. VI. Section VII contains the summary and conclusions of this paper.

II. ALGORITHM OF MONTE CARLO SIMULATIONS

The bond fluctuation model is an efficient method of simulating the dynamics of large numbers of polymer chains. It was originally introduced by Carmesin and Kremer [14] for studying dynamics of polymer chains in various spatial dimensions. Since then it has been used for investigation of the crossover between Rouse and reptation dynamics [15], for studying interdiffusion of polymer blends [16], the dynamics of polymer melts near glass transition [17], and polymer crystallization in dilute solution [18].

Each monomer in the model occupies a $2\times2\times2$ cube of

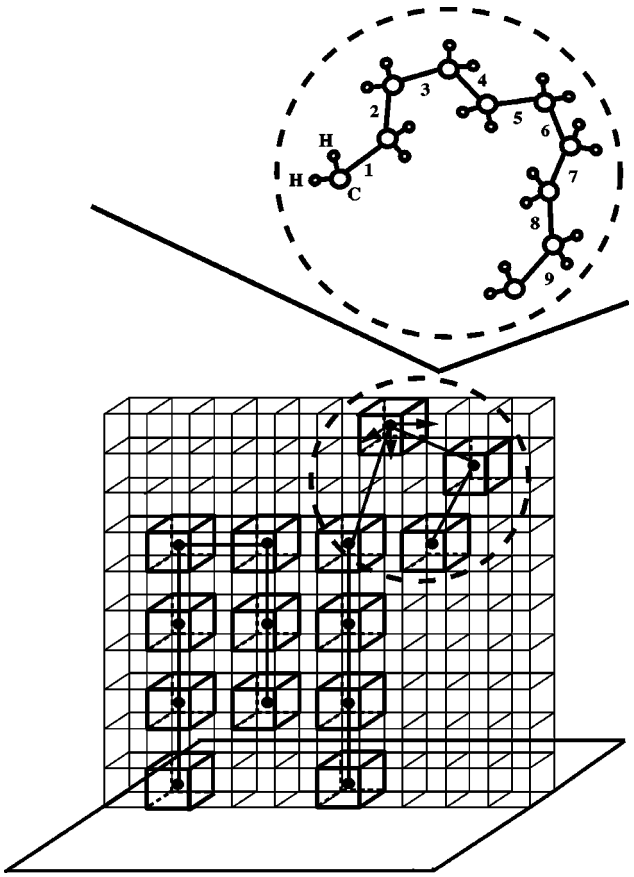

FIG. 1. Two chains of seven monomers are shown. All monomers are shown in one plane for convenience although the simulations are done in three dimensions. Each bond in our model is equivalent to the persistent length of polymer chains, which contains several real bonds.

sites on a cubic lattice as shown in Fig. 1. The set of allowed bond vectors is

$$\mathbf{B}=P(2,0,0)\cup P(2,1,0)\cup P(2,1,1)\cup P(2,2,1)\cup P(3,0,0)\cup P(3,1,0), \quad (1)$$

where $P(a,b,c)$ stands for the set of all permutations and sign combinations of $\pm a,\pm b,\pm c$. The number of configurations per bond is $z=108$. The length of one bond can take any one of the five values $\sqrt{2},\sqrt{5},\sqrt{6},\sqrt{3},\sqrt{10}$ (in units of lattice spacing). Chains satisfy the excluded volume constraint: no lattice site may be occupied by more than one monomer. Each attempted move is to move one monomer by one lattice site in one of the six lattice directions. The move is rejected if the new position breaks the excluded volume constraint, or if the new bond vectors between the monomer which was moved and its neighbors are not contained in the set **B**. The set **B** is chosen to satisfy the constraints of both excluded volume between monomers and topological entanglement between chains (i.e., two chains cannot pass through each other). If any other bond vectors were added to this set, some chains would become ''phantom'' chains.

Since semiflexible polymer chains have a longer persistent length than flexible polymers, we have added a bond-bond interaction between two parallel neighboring bonds instead of a monomer-monomer interaction between two neighboring monomers. This is modeled by an energy -1 unit if it is an attractive interaction (in poor solvents) or 1 unit if it is a repulsive interaction (in good solvents) whenever there are two parallel bonds (nonsuccessive) on neighboring sites. In addition, in our model, there is a bending energy of $e(1-\cos\theta)$ for two successive bonds with a bond angle θ, where e is the bending rigidity. We note that the average bond-bond interaction is much smaller than the average bending energy for $e\sim 1$ since the probability of two bonds in parallel is quite small. Therefore, the effects of bond-bond interaction have been ignored in this paper.

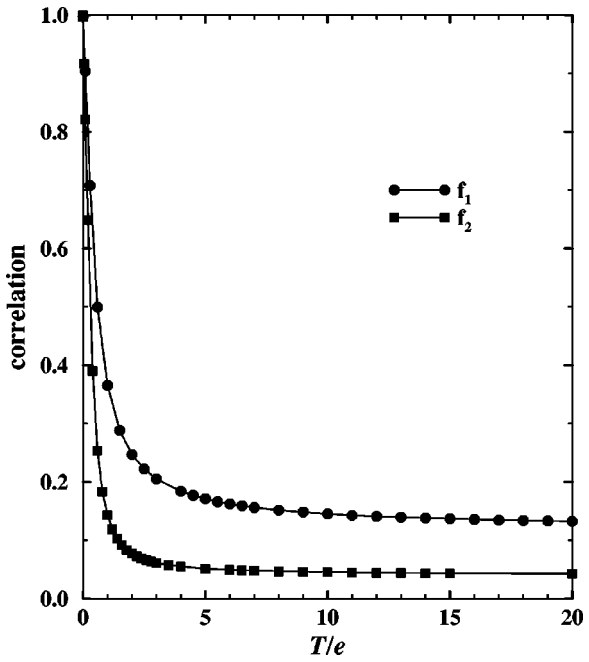

FIG. 2. Angular correlations between nearest neighboring bonds (f_1) and next nearest neighboring bonds (f_2) as a function as T/e. For $T/e>5$, both correlations are not affected by the stiffness parameter e. For $T/e<5$, polymer chains are less flexible or more persistent.

Simulations are carried out at a constant temperature T using the Metropolis algorithm. If any attempted move of monomers satisfies the excluded volume constraint and the new bond vectors are still in the allowed set, then the move is accepted with probability

$$w=\min[1,\exp(-\Delta E/T)], \quad (2)$$

where ΔE is the energy change. The two parameters in the model are the temperature T and the bending rigidity e. If $T/e\gg 1$ and T is not much less than 1, the chain behaves as a self-avoiding walk. If $T/e\ll 1$ the chain will be rodlike. In order to determine appropriate parameter ranges for the simulations, we measured the angular correlations between nearest neighboring bonds (f_1) and next nearest neighboring bonds (f_2) as a function of T/e (as shown in Fig. 2), where $f_1\equiv\langle \mathbf{u}_i\cdot\mathbf{u}_{i+1}\rangle_{\mathrm{en}}$, $f_2\equiv\langle \mathbf{u}_i\cdot\mathbf{u}_{i+2}\rangle_{\mathrm{en}}$, and $\mathbf{u}_i$ is the unit vector of the ith bond. The angular bracket $\langle\ \rangle_{\mathrm{en}}$ indicates an en-

semble average over all possible configurations weighted by their Boltzmann probabilities. Figure 2 shows that for $T/e > 5$ there is almost no change in these correlations. Both f_1 and f_2 have small positive values at large T/e which are due to excluded volume constraints only but not the bending energy term. For $0.5 < T/e < 5$ the chain is significantly stiffened by the bending energy term and thus corresponding to semiflexible polymer chains. In all simulations presented in this paper $0.5 < T/e$ so that the chains in solution behave like flexible or semiflexible self-avoiding walks.

The simulated polymer brush is randomly grafted on a flat substrate of area 30×30 and a periodic boundary condition is applied. Each polymer chain is initially perpendicular to the substrate and later allowed to relax to its equilibrium state such that the average end-to-end distance of the chain reaches an equilibrium value. After the equilibrium is reached, we then perform a long simulation to calculate the monomer density distribution, end density distribution, end-to-end distance, angular distribution, and orientation order parameter S for various values of grafting density, chain length, and bending rigidity. The monomer and end density distributions have been averaged every two layers in the z direction to eliminate the lattice effects. Thus in the following paragraphs of this paper, we will use two lattice spacings as the unit of length in the z direction.

III. EQUILIBRIUM STRUCTURE OF POLYMER BRUSHES

The equilibrium structure of flexible polymer brushes has been an attractive research topic for many years. Alexander [2] and de Gennes [3] first proposed the so-called Flory argument which estimates the average brush height (h) by balancing the configurational entropy of polymer chains and the excluded interaction between monomers based on a step function ansatz of monomer density distribution. More specifically, $h \sim N(w\sigma a^2)^{1/3}$, where Na is the chain length of polymers, w is the excluded volume parameter, and σ is the grafting density. Later Milner, Witten, and Cates [4] presented a more detailed self-consistent field (SCF) theory of polymer brushes. Instead of assuming a step function of monomer density distribution, SCF predicts a ''parabolic'' brush whose monomer density $[\phi(z)]$ and end density $[\epsilon(z)]$ along the substrate normal direction (z direction) can be expressed as

$$\frac{\phi(z)}{\sigma^{2/3}} = \frac{\pi^2}{8w}(H^2 - Z^2)\,\theta(H-Z) \tag{3}$$

and

$$\frac{\epsilon(z)N}{\sigma^{2/3}} = \frac{\pi^2}{2w} Z (H^2 - Z^2)^{1/2} \theta(H-Z), \tag{4}$$

where $H = h/(N\sigma^{1/3})$ and $Z = z/(N\sigma^{1/3})$ are rescaled brush height and distance away from the substrate, and $\theta(z)$ is the step function.

To compare our simulation results with the predictions of SCF, we plot the rescaled monomer density distribution and

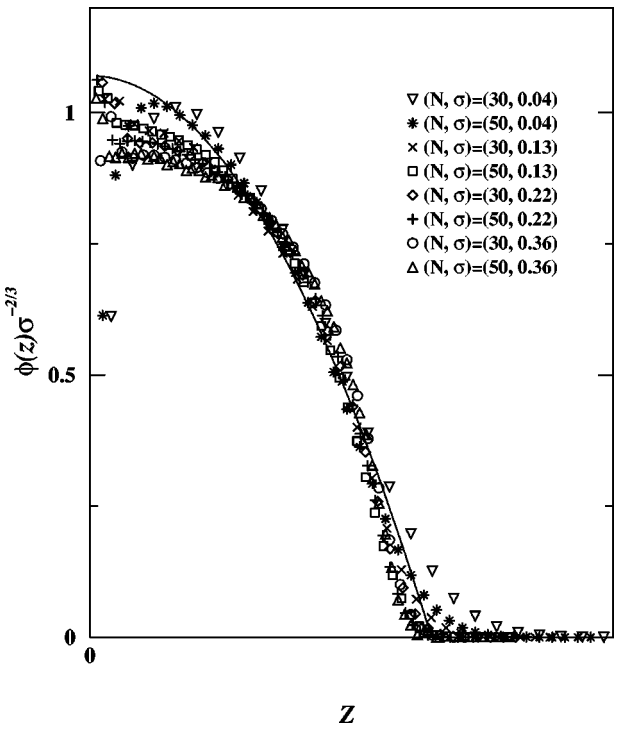

FIG. 3. Rescaled monomer density distributions of polymer brushes along the z direction for $T/e = 7.5$ and $(N,\sigma) = (30,0.04)$, (50,0.04), (30,0.13), (50,0.13), (30,0.22), (50,0.22), (30,0.36), and (50,0.36). The solid line is a theoretical curve of SCF. Here Z is defined as $zN^{-1}\sigma^{-1/3}$.

end density distribution for $e = 1.0$ and $T = 7.5$ ($T/e = 7.5$ is in the flexible regime) in Figs. 3 and 4 which qualitatively fit theoretical curves (solid lines) of Eqs. (3) and (4). As shown in Fig. 3, apart from the regions close to the substrate and the tail of the profiles, our simulated data collapses reasonably well onto a universal curve as predicted by SCF. The exponential tail of monomer density profile is, however, in agreement with the prediction of SCF for finite chains [1,7]. The length scale of the tail relative to the brush height decreases with chain length and grafting density and is vanishingly small at the long chain limit. Near the substrate, our Monte Carlo data show a depletion layer [3,7] at low grafting densities ($\sigma < 0.09$) but an enhancement in the monomer density at medium grafting densities ($\sigma > 0.1$). This enhancement has been confirmed by performing several long Monte Carlo simulations. To further investigate the difference in monomer density at different grafting densities, in Figs. 5(a) and 5(b), we show the monomer density distribution at different time steps after releasing the brushes from their initial configuration. As shown in Figs. 5(a) ($\sigma = 0.02$) and 5(b) ($\sigma = 0.22$), the polymer chains shrink to increase the system entropy and two peaks are observed near the substrate and at the brush tail. As time increases, both peaks grow [the outer peak grows faster in (a) than in (b)] and the outer peak moves toward the substrate. Finally, the outer peak stops before reaching the substrate. As a result, near the substrate, we observe a depletion layer in (a) for low grafting densities but an enhancement layer in (b) for medium grafting densities. We conclude that polymer brushs at a medium grafting

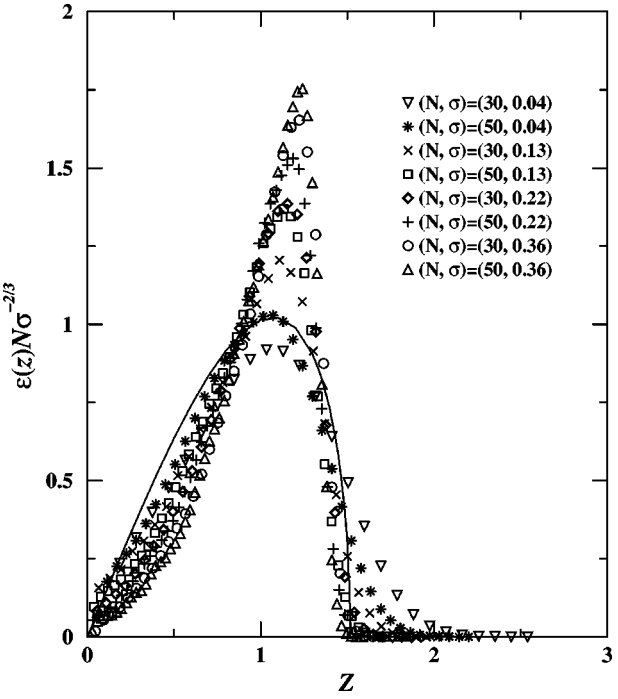

FIG. 4. Rescaled end density distributions of polymer brushes along the z direction for $T/e=7.5$ and $(N,\sigma)=(30,0.04)$, (50, 0.04), (30,0.13), (50,0.13), (30,0.22), (50,0.22), (30,0.36), and (50,0.36). The solid line is a theoretical curve of SCF. Here Z is defined as $zN^{-1}\sigma^{-1/3}$.

density strongly compress near the substrate to increase the entropy of the system. The agreement in the end density between theoretical predictions and our simulated data is only good at the limit of long chain length and low grafting density, as shown in Fig. 4. For short chains, the exponential tail is significant. At medium grafting densities, the peak of end density distribution is much sharper than that predicted by SCF. In this case, the end density is suppressed in the inner region due to high monomer density.

The brush height of a polymer brush can be measured from the monomer density distribution by fitting Eq. (3). For flexible polymers, theoretical prediction of the brush height ($h_f \propto N\sigma^{\beta}$ where $\beta=1/3$) is found to be in great agreement with simulation results at the limit of long chains. For short chains, the brush height is roughly proportional to $\sigma^{1/4}$ or $\beta\simeq 0.25$, indicating that nonlinear stretching of polymer chains becomes significant and one can express the stretching energy as $f_{\text{stretching}}\propto h^3$ for $N\sim 10$. A list of the values of β for various chain lengths is given in Table I. For semiflexible polymer brushes, the brush height (h_{sf}) is expected to be longer than that of flexible brushes due to the bending energy and we have $h_{\text{sf}}=h_e+h_f$, where h_e is the correction of brush height due to bending energy. The dependence of brush height (h_{sf}) on the chain stiffness and temperature is shown in Fig. 6 for $(N,\sigma)=(20,0.22)$ (a), (40, 0.22) (b), and (60, 0.22) (c). The intercept of those curves with the y axis in Fig. 6 gives the brush height of flexible brushes. It is clear from Fig. 6 that h_e is proportional to e/T and N. Further investigation shows no dependence of h_e on the grafting density. From our Monte Carlo simulation results, we can express the brush height of semiflexible brushes as

$$h_{sf}\simeq k_1\frac{e}{T}N+k_2N\sigma^{\beta}, \tag{5}$$

where $k_1\simeq 0.11$ and $k_2\simeq 1.38$. Therefore, the correction of brush height due to chain stiffness is about one tenth. Similar analyses can be done for the end-to-end distance (l_{sf}) of each chain as shown in Fig. 7 and we conclude an expression of l_{sf} as

TABLE I. The values of β, γ, and δ for various chain lengths.

N	20	40	60
β	0.27	0.31	0.32
γ	0.17	0.28	0.31
δ	0.24	0.32	0.34

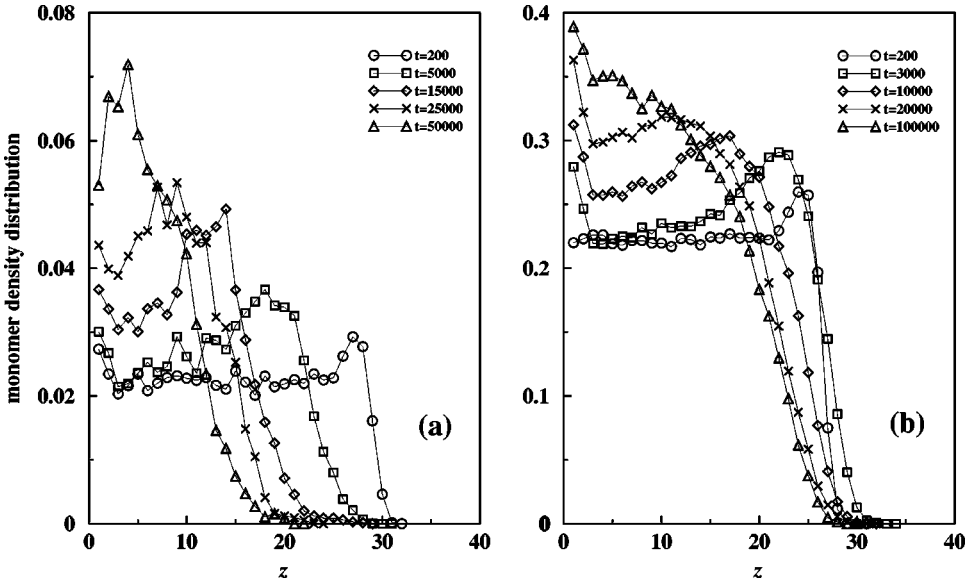

FIG. 5. Monomer density distributions of polymer brushes along the z direction for $T/e=7.5$, $N=30$ at various time steps. Time (t) is in units of Monte-Carlo steps. The grafting density is 0.02 (a) and 0.22 (b).

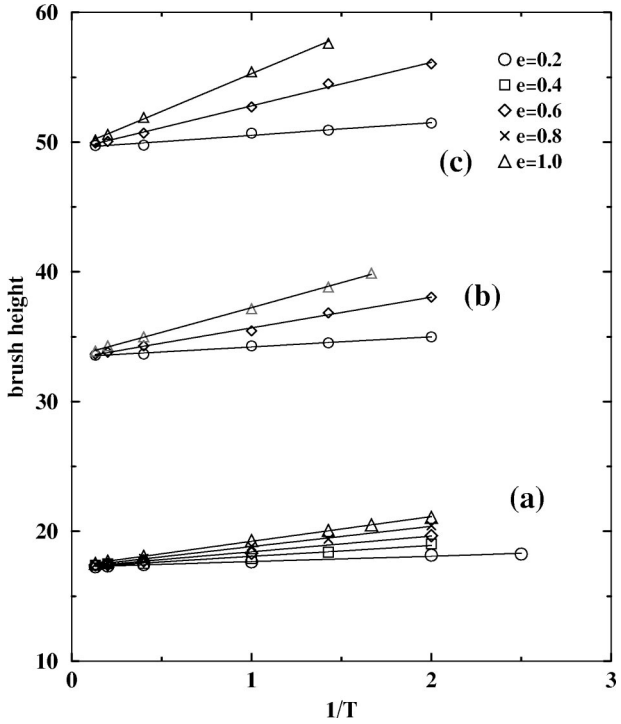

FIG. 6. The dependence of brush height of semi-flexible polymer brushes on the bending rigidity and temperature for $(N,\sigma)=(20,0.22)$ (a), (40,0.22) (b), and (60,0.22) (c).

$$l_{sf} \simeq k_3 \frac{e}{T} N\sigma^{\gamma} + k_4 N\sigma^{\delta}, \tag{6}$$

where $k_3 \simeq 0.21$, $k_4 \simeq 2.1$, and the values of γ and δ are given in Table I. Unlike Eq. (5), Eq. (6) shows a dependence of the correction to end-to-end distance on the grafting density (σ^{γ}) and γ increases with N. In the appendix, we present a simple scaling argument for Eqs. (5) and (6).

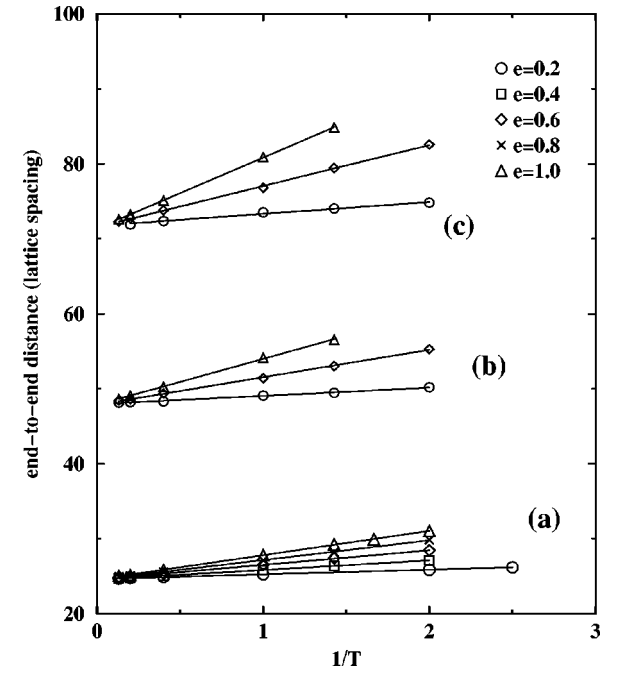

FIG. 7. The dependence of end-to-end distance of semi-flexible polymer brushes on the bending rigidity and temperature for $(N,\sigma)=(20,0.22)$ (a), (40,0.22) (b), and (60,0.22) (c).

IV. DISTRIBUTION OF BENDING ANGLES

To further analyze equilibrium properties of polymer brushes, we study the change in the bending angle distribution as temperature varies. For an equilibrated brush, the distribution of bending angles at high temperatures is uniform except for large angles due to the excluded volume constraint (no overlaps between monomers). As temperature decreases, the angular distribution is expected to be more weighted at small angles and there exists an unbiased angle (θ_u) whose weighting does not change with temperature. Since the probability of a bending angle is proportional to its Boltzmann factor, we can express the weighting of the ith angle at temperature T as

$$P_i(T) = \frac{1}{N_a} \exp\left(\frac{\alpha_i}{T}\right), \tag{7}$$

where N_a is the number of allowed angles, $\alpha_i = E_u - E_i$ is the weighting factor, E_u is the energy of the unbiased angle, and E_i is the energy of the ith angle. To determine the unbiased angle, we can substitute it by anyone of those N_a angles and check if the normalization condition $\Sigma_{i=1}^{Na} P_i(T) = 1$ holds at various temperatures. Assuming that the energy of a polymer chain is dominated by the bending energy, we can calculate the corresponding spectrum of weighting factor for a particular form of bending energy. Here, four different forms of bending energy are used to investigate the spectrum and they are expressed in the following:

$$\begin{aligned} E_B^{\text{cosine}} &= e(1-\cos\theta), \\ E_B^{\text{linear}} &= 2e(\theta/\pi), \\ E_B^{\text{quadric}} &= 2e(\theta/\pi)^2, \\ E_B^{\text{quartic}} &= 2e(\theta/\pi)^4, \end{aligned} \tag{8}$$

where the range of θ is chosen to be between 0° and 144° in order to compare with our simulation results using the bond fluctuation model (no overlaps between monomers rules out angles larger than 144°). If we divide the range of θ into 145 angles, the unbiased angle can be obtained by varying the spectrum of weighting factor $\{\alpha_i\}$ subject to the normalization condition $\Sigma_{i=1}^{Na} P_i(T) = 1$ at various temperatures, which is found to be 75° for E_B^{cosine},72° for E_B^{linear},84° for E_B^{quadric}, and 96° for E_B^{quartic}. It is obvious that the unbiased angle for a linear bending energy is 72° which is at the middle of the angular range. For the other three asymmetric forms of bending energy, the unbiased angle is shifted to larger values. The angular distribution can be calculated at any temperature from $\{\alpha_i\}$ and is displayed in Fig. 8 for $T/e = 1$. The agreement between the theoretical curve and our simulation data of the cosine form is excellent. We note that, for $T/e \lesssim 1$, the

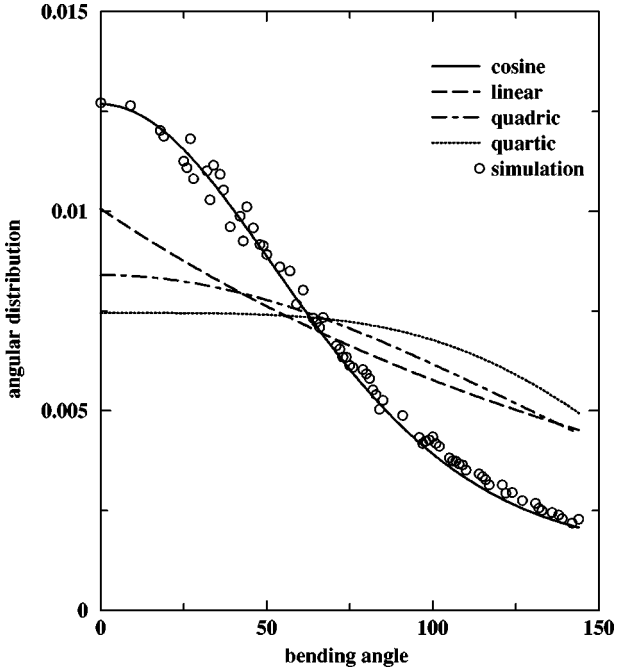

FIG. 8. Theoretical predictions of the distribution of bending angles of a polymer brush at $e/T=1$ for four different forms of bending energy. The angular distribution of the cosine form is much more populated at small bending angles. Open circles are simulation data of the cosine form.

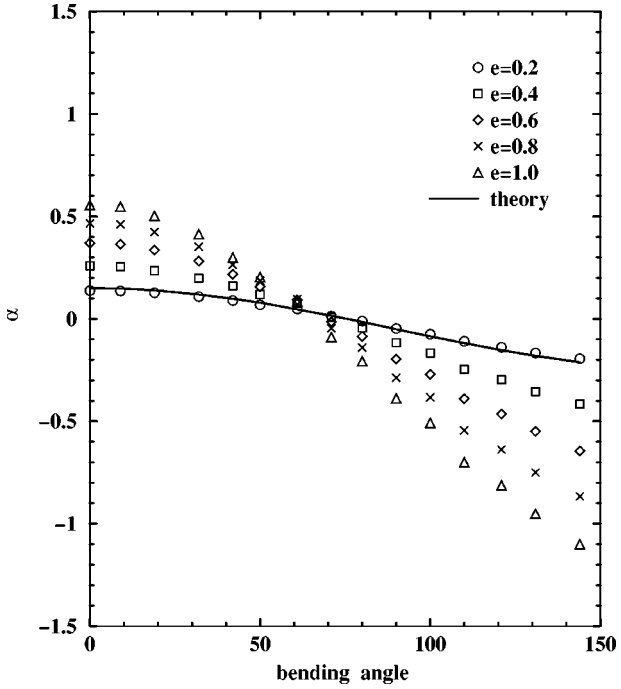

FIG. 9. The spectrum of weighting factor $\{\alpha_i\}$ for $e=0.2$ (○), 0.4 (□), 0.6 (◇), 0.8 (×), and 1 (△) using the cosine form of bending energy. The solid line is a theoretical curve for $e=0.2$.

unbiased angle calculated deviates from the above predicted values and one should expect a slightly modified angular distribution.

The distribution of bending angles can also be measured at various temperatures in our simulations from which the spectrum of weighting factor is obtained. In our model, if we divide the range of θ into 180 units, there are 72 allowed bending angles and the maximum is 144°. To remove the lattice effects, we rescale the angular distribution at temperature T by dividing it by the distribution at infinite temperature such that the rescaled distribution is uniform at high temperatures. The calculated spectrum $\{\alpha_i\}$ using the bond fluctuation model for $\sigma=0.22$ and $N=20$ is shown in Fig. 9 where only part of data points are shown. The solid line is a theoretical curve predicted by $\alpha_i=e(\cos\theta_i-\cos\theta_u)$ with $e=0.2$ and $\theta_u=75°$, which fits our simulation data (circles) very well. Moreover, from Fig. 8 it is clear that small bending angles are more populated for the cosine form of bending energy than for other forms, and we expect the degree of stretching of polymer chains to be cosine>linear>quadric>quartic. In Fig. 10, we show the monomer density distribution for $\sigma=0.22$, $N=50$, and $T/e=1$ using four different forms of bending energy. The above prediction is confirmed by the fact that the brush height is in the sequence of cosine>linear>quadric>quartic.

V. ISOTROPIC TO NEMATIC PHASE TRANSITION

The isotropic-nematic phase transition of polymer systems is also an interesting subject and attracts much attention [19,5]. To describe such a phase transition in a polymer brush, it is convenient to define an order parameter $S\equiv(3\langle\cos^2\omega\rangle_{en}-1)/2$ to characterize the orientational ordering, where ω is the angle between orientation of a segment and the normal to the substrate (i.e., the z direction). To view

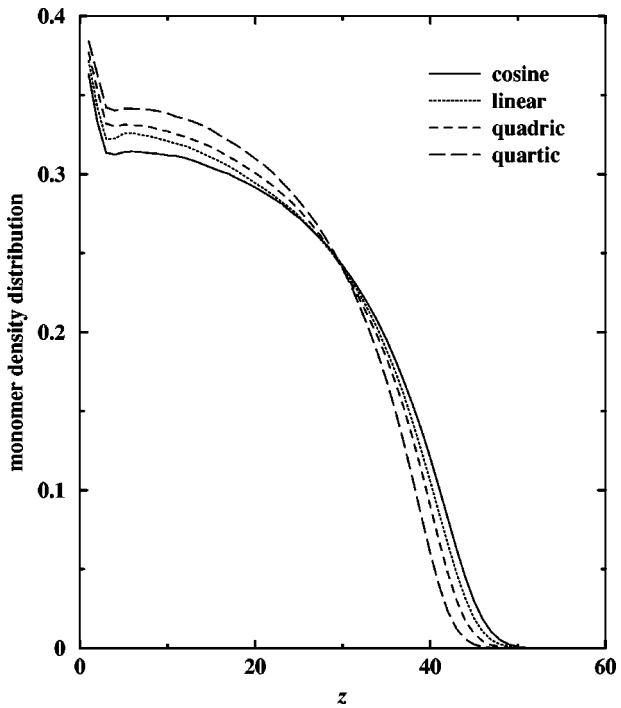

FIG. 10. The monomer density distribution of a polymer brush for $\sigma=0.22$, $N=50$, and $e/T=1$ for four different forms of bending energy.

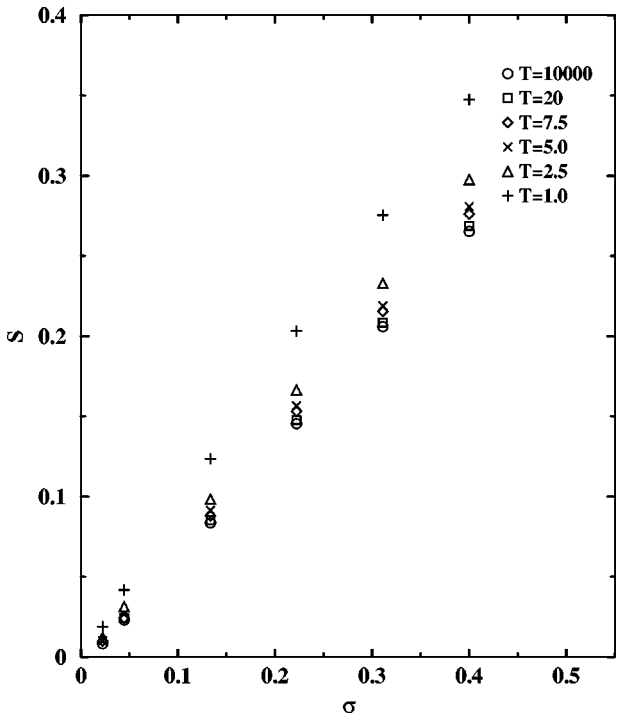

FIG. 11. The order parameter S as a function of σ for $N=20$ and $e=1$ at various temperatures. A continuous isotropic-nematic phase transition occurs at a small grafting density ($\sigma<0.02$).

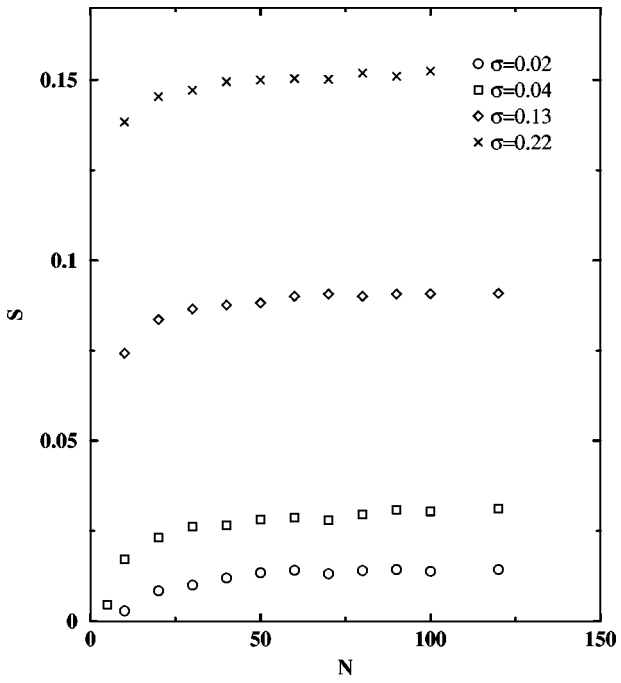

FIG. 12. The order parameter S as a function of N for $T=10\,000$ and $e=1$ at various grafting densities. S is almost a constant for large chain lengths and is smaller for small chain length since the polymer chains behave as ''nonlinear'' springs for small N.

this phase transition in a simple way, we consider a free energy per chain composed of an anisotropic interaction energy ($f_{\text{anisotropy}}$) and an orientational free energy ($f_{\text{orientation}}$). This anisotropic interaction energy could come from the nematic interaction between two persistent segments or the bending energy between two consecutive segments and is assumed to have a power series expansion in S,

$$f_{\text{anisotropy}} \sim \text{const} - uNS^2 + \cdots, \tag{9}$$

where $u=u(e,\sigma)$ is the coefficient of anisotropic interactions and always positive since both the bending energy and segment-segment interaction tend to align a polymer chain along the z direction. The orientation free energy can be approximated in the following form as suggested by Kuznetsov and Chen [5]:

$$f_{\text{orientation}} \sim \frac{N(2S+1)}{1-\left(\frac{2S+1}{3}\right)^{1/3}} + \text{const.} \tag{10}$$

Such a free energy ($f_{\text{anisotropy}}+f_{\text{orientation}}$) can be easily minimized to find the ground state and the isotropic-nematic transition is expected to be a first order phase transition.

To examine this simple theory, we have performed many simulations to study the phase transition of polymer brushes from an isotropic state to a nematic state by varying the bending rigidity, grafting density, temperature, and chain length. As shown in Fig. 11, the order parameter S increases linearly from zero as the grafting density increases for $T/e=1$, 2.5, 5, 7.5, 20, and 10 000. The isotropic phase occurs only at very low grafting densities ($\sigma<0.02$) and the isotropic-nematic phase transition is possible to be continuous. It is clear that the above simple model cannot describe the isotropic-nematic phase transition of polymer brushes and a more accurate model is desired. Moreover, as shown in the previous section, the orientation free energy in Eq. (10) is incorrect at the short chain limit and in this limit polymer chains behave as ''nonlinear'' springs which favor an isotropic phase over a nematic phase. In Fig. 12, we show the order parameter S as a function of chain length N. Our results show that S is almost a constant for long chain lengths and becomes smaller as N decreases. In addition, the order parameter S increases with the grafting density at a very high temperature ($T=10\,000$) which indicates that the excluded volume effect is the dominant source to drive the system to a nematic phase in our model.

VI. EFFECTS OF LOCAL GRAFTING DENSITY FLUCTUATION

In previous sections, we have studied the equilibrium structure of randomly grafted polymer brushes without worrying the effects of local grafting density fluctuation. However, it is inevitable to face questions about the fluctuation effects and their importance. For example, it would be difficult and expensive to grow polymer brushes with an uniform grafting density in industrial applications. To investigate the effects of local grafting density fluctuation, we measure the monomer and end density distributions for polymer brushes of the same average density but different variance. Here the variance of grafting density is defined as $v=\sqrt{\langle(\sigma_i/\sigma-1)^2\rangle}$, where σ is the average grafting density,

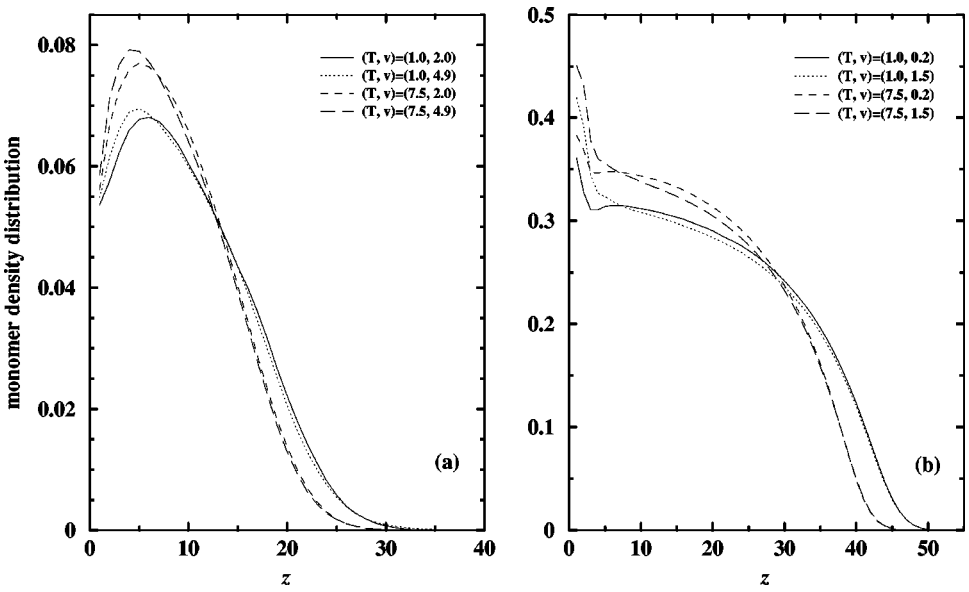

FIG. 13. The monomer density distribution of polymer brushes at various v and T for (a) $\sigma=0.02$ and (b) $\sigma=0.22$. The polymer chain length is $N=50$ and the bending rigidity is $e=1$.

σ_i is the local grafting density at the ith patch, and the substrate is divided into 25 patches of same area. The monomer density distributions of flexible ($T/e=7.5$) and semiflexible ($T/e=1$) polymer brushes of chain length $N=50$ are shown in Fig. 13 for $\sigma=0.02$ (a) and $\sigma=0.22$ (b). From Fig. 13, it is clear that the effects of local grafting density fluctuation on the monomer density distribution are insignificant and therefore we only show two sets of data ($v=2$ and 4.9). To be more specific, we find that the monomer density is slightly enhanced near the substrate for a larger local grafting density fluctuation. This enhancement is because polymer chains in a denser region tend to repel each other strongly due to the exclude volume effect, particularly for those monomers near the fixed ends, and these monomers can only be bent to less dense regions near the substrate. This phenomenon is true for both flexible and semiflexible brushes at various grafting densities. However, for small grafting densities the brush height is slightly reduced in the case of a larger fluctuation, but the brush height for medium grafting densities is not affected since it is more difficult for those monomers in the outer region to move in due to a larger monomer density. Similarly the end density in the inner region is enhanced for a larger fluctuation as shown in Figs. 14(a) ($\sigma=0.02$) and 14(b) ($\sigma=0.22$). The reason for this enhancement of the end density in the inner region is because fluctuation tends to reduce the monomer density in the outer region and makes it easier for the end monomers to move toward the substrate.

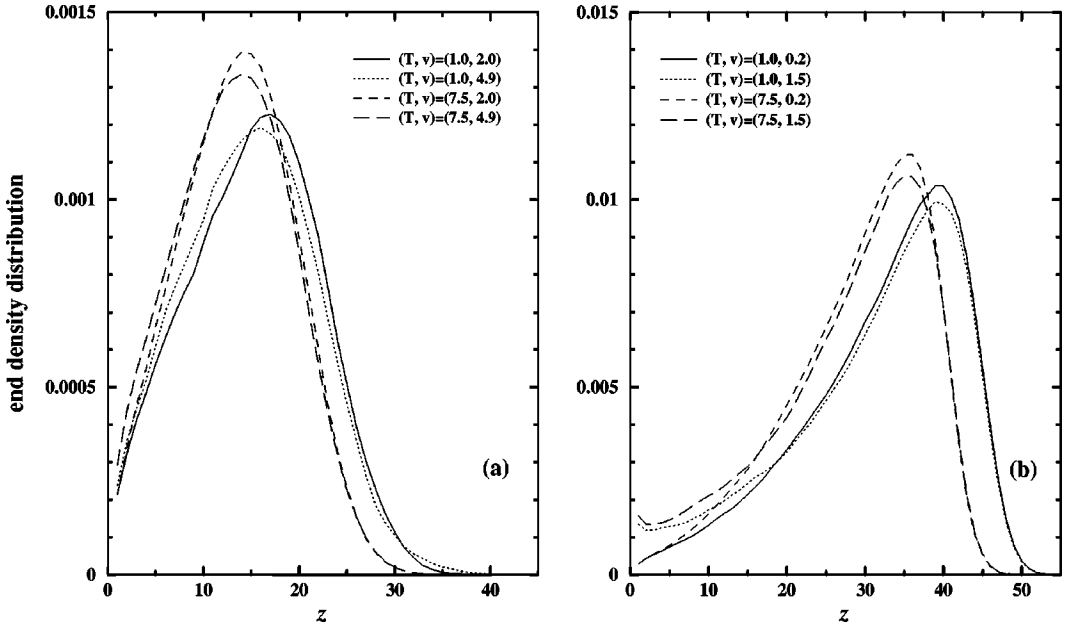

FIG. 14. The end density distribution of polymer brushes at various v and T for (a) $\sigma=0.02$ and (b) $\sigma=0.22$. The polymer chain length is $N=50$ and the bending rigidity is $e=1$.

VII. SUMMARY AND CONCLUSIONS

To summarize, we have used the bond fluctuation model to study various equilibrium properties of flexible and semiflexible polymer brushes in great detail. Significant improvement toward understanding polymer brushes has been made in this paper. For flexible brushes, our simulation results are in general consistent with theoretical predictions of SCF. However, the depletion layer near the substrate is only observed at low grafting densities, and the monomer density near the substrate is enhanced at medium grafting densities due to a strong compression of polymer chains. Note that, although the grafting density in our simulations is up to 0.36, we have not seen the Pincus regime where polymer chains are strongly stretched [20]. For semiflexible polymer brushes, we find that the correction of brush height due to the bending energy is proportional to Ne/T, and is only about one tenth of the brush height. Interestingly, we find that the correction of end-to-end distance due to bending rigidity is also one tenth of the end-to-end distance, but this correction has a dependence on σ which needs a theoretical explanation. Moreover, the distribution of bending angles of polymer brushes is analyzed at various temperatures. Four different forms of the bending energy are used to study the angular distribution and their corresponding unbiased angles are calculated. Compared with our simulation results, we find excellent agreement for the spectrum of weighting factor $\{\alpha_i\}$. In addition, we have also investigated the isotropic to nematic phase transition of polymer brushes. From our simulations, we find that this phase transition is controlled by the excluded volume effect (or the grafting density) and the bending energy has very little effect on the transition. In contrast to a first order phase transition predicted by a simple model, we find a possible second order isotropic-nematic transition at a very small grafting density. Furthermore, for short polymer chains, the nonlinear effect is found to favor the isotropic phase over the nematic phase. Finally, we have studied the effects of local grafting density fluctuation. For large fluctuation, both monomer density and end density are enhanced near the substrate at various grafting densities and temperatures. However, these effects are small and can possibly be ignored in industrial applications.

ACKNOWLEDGMENTS

We are grateful to Dr. P.-Y. Lai and Dr. M. Zuckermann for their useful suggestions and comments on our work. The authors acknowledge the support from NSC of Taiwan under Grant No. 89-2112-M-003-001.

APPENDIX: SCALING OF END-TO-END DISTANCE OF SEMIFLEXIBLE POLYMER BRUSHES

The end-to-end distance (l) of long flexible chains of N segments is known to be $\sqrt{N}a$, where a is the Kuhn length. For semi-flexible polymer chains, the mean square end-to-end distance can be written as

$$\begin{aligned} l_{sf}^2 &= \left\langle \left(\sum_{i=1}^{N} \mathbf{r}_i \right) \left(\sum_{j=1}^{N} \mathbf{r}_j \right) \right\rangle \\ &= Na^2 + 2 \left\langle \sum_{i=1}^{N-1} \sum_{j=i+1}^{N} \mathbf{r}_i \cdot \mathbf{r}_j \right\rangle \\ &\simeq l^2 + 2 \left\langle \sum_{i=1}^{N-1} \mathbf{r}_i \cdot \mathbf{r}_{i+1} \right\rangle, \end{aligned} \tag{A1}$$

for small bending rigidity e, where $\mathbf{r}_i$ is the bond vector of the ith segment. For the cosine form of bending energy, the nearest bond-bond correlation can be calculated as

$$\begin{aligned} \langle \mathbf{r}_i \cdot \mathbf{r}_{i+1} \rangle &\equiv a^2 \int \cos\theta \exp\left[-\frac{e}{T}(1-\cos\theta) \right] d\theta \\ &\simeq \frac{\pi e}{2T} a^2. \end{aligned} \tag{A2}$$

Therefore the mean square end-to-end distance of a semiflexible chain is $l_{sf}^2 \sim (1+e/T) l^2$. Rescaling the length by a factor $1-e/(2T)$, the free energy of a semiflexible brush can be written as

$$F \sim \frac{N^2 \sigma}{l_{sf}\left(1-\frac{e}{2T}\right)} + \frac{l_{sf}^2\left(1-\frac{e}{T}\right)}{N}. \tag{A3}$$

Minimizing Eq. (A3) with respect to l_{sf}, we obtain

$$l_{sf} \sim N\sigma^{1/3}\left(1+\frac{e}{T}\right), \tag{A4}$$

which is consistent with Eq. (6) in the long chain limit. We note a difference between Eqs. (5) and (6) in the σ dependence of the correction part due to bending rigidity. It is possible that rescaling of brush height might have a dependence on σ which cancels the σ dependence of the correction part in Eq. (5). A more complete theory would be required to resolve this difference.

[1] S. T. Milner, Science **251**, 905 (1991).
[2] S. Alexander, J. Phys. (France) **38**, 983 (1977).
[3] P. G. de Gennes, Macromolecules **13**, 1069 (1980).
[4] S. T. Milner, T. A. Witten, and M. E. Cates, Macromolecules **21**, 2610 (1988).
[5] D. V. Kuznetsov and Z. Y. Chen, J. Chem. Phys. **109**, 7017 (1998).
[6] P. Y. Lai and K. Binder, J. Chem. Phys. **98**, 2366 (1993); I. M. Neelov, O. V. Borisov, and K. Binder, *ibid.* **108**, 6973 (1998); A. Milchev, J. P. Wittmer, and D. P. Landau, *ibid.* **112**, 1606 (2000).
[7] M. Laradji, H. Guo, and M. J. Zuckermann, Phys. Rev. E **49**, 3199 (1994).
[8] A. Karim *et al.*, Phys. Rev. Lett. **73**, 3407 (1994); S. Forster,

E. Wenz, and P. Lindner, *ibid.* **77**, 95 (1996).
[9] T. Hu and C. Wu, Phys. Rev. Lett. **83**, 4105 (1999).
[10] M. Daoud and J. P. Cotton, J. Phys. (Paris) **43**, 531 (1982).
[11] H. Chen and A. Chakrabarti, Phys. Rev. E **52**, 3915 (1995).
[12] G. T. Pickett and T. A. Witten, Macromolecules **25**, 4569 (1992); B. Li and E. Ruckenstein, J. Chem. Phys. **106**, 280 (1997).
[13] C. M. Wijmans, F. A. M. Leermakers, and G. J. Fleer, J. Chem. Phys. **101**, 8214 (1994).
[14] I. Carmesin and K. Kremer, Macromolecules **21**, 2819 (1988).
[15] I. Gerroff, A. Milchev, K. Binder, and W. Paul, J. Chem. Phys. **98**, 6526 (1993).
[16] H. P. Deutsch and K. Binder, J. Chem. Phys. **94**, 2294 (1991).
[17] P. Ray, J. Baschnagel, and K. Binder, J. Phys.: Condens. Matter **5**, 5731 (1993).
[18] C.-M. Chen and P. G. Higgs, J. Chem. Phys. **108**, 4305 (1998).
[19] A. R. Khokhlov and A. N. Semenov, Physica A **108**, 546 (1981).
[20] P. Pincus, Macromolecules **9**, 386 (1976); J. T. Titantah, C. Pierleoni, and J.-P. Ryckaert, Phys. Rev. E **60**, 7010 (1999).